Henry's Constant Analysis for Water and Nonpolar Solvents from Experimental Data, Macroscopic Models, and Molecular Simulation

Georgios C. Boulougouris,[†,‡] Epaminondas C. Voutsas,[‡] Ioannis G. Economou,*[,†] Doros N. Theodorou,[†,§] and Dimitrios P. Tassios[‡]

Molecular Modeling of Materials Laboratory, Institute of Physical Chemistry, National Research Centre for Physical Sciences ''Demokritos'', GR-15310 Aghia Paraskevi Attikis, Greece, Thermodynamics and Transport Phenomena Laboratory, Department of Chemical Engineering—Section II, National Technical University of Athens, 9 Heroon Polytechniou Str., Zographos GR-15780, Athens, Greece, and Department of Chemical Engineering, University of Patras, GR-26500 Patras, Greece

Received: February 5, 2001; In Final Form: May 20, 2001

Experimental data, equations of state (EoS), and Monte Carlo simulations are used to analyze the Henry's law constant of solutes in water and in organic solvents at different temperatures. EoS are incapable of correlating the experimental data for light hydrocarbons dissolved in water. Novel simulation methodologies are used for methane in water and in ethane. Results are analyzed with respect to the free energy of cavity formation for hosting the solute molecule in the solvent and the free energy of interactions between the solute molecule and the solvent. It is shown that the hydrophobic phenomenon is driven, to a large extent, by the weak intermolecular interactions between water molecules and nonpolar solute molecules.

Introduction

The Henry's law constant is used widely to describe the low solubility of light solutes in a variety of solvents at relatively low pressure over a wide temperature range.[1−3] Experimental data and accurate correlations have been reported for many solutes in different solvents such as water,[1] light and heavy hydrocarbons,[2,3] and others.[2] Typically Henry's constant increases with temperature for relatively low-temperature values, goes through a maximum, and then decreases for higher temperatures. A relatively high Henry's constant value corresponds to low solubility and vice versa. Traditionally, the low solubility of a solute in a solvent has been associated with differences in energetic interactions between solvent molecules and solute molecules or differences in molecular size or both. A typical example of the first case is the dissolution of *n*-alkanes in water. *N*-alkane molecules interact through weak London forces, whereas water molecules exhibit strong hydrogen-bonding interactions resulting in three-dimensional structures. A representative example for the second case is that of light gases (hydrogen, nitrogen, etc.) dissolved in a heavy *n*-alkane.

In this work, a generalized thermodynamic framework is presented for the analysis of the Henry's constant and its variation with temperature. Henry's constant is expressed as a product of two terms: The first term involves pure solvent thermodynamic properties only. The second term is a function of the excess chemical potential of the solute at the state conditions examined. The latter is subdivided into a term associated with the formation of a cavity in the solvent to host the solute molecule and a term that accounts for the free energy of inserting the solute into the cavity by turning on the energetic interactions between solute and solvent molecules. In this way, detailed analysis of the various factors affecting Henry's constant is performed. Experimental data for two representative systems, methane in water[3] and methane in *n*-hexadecane,[3] are analyzed according to the proposed scheme.

Mixture phase equilibrium data are often correlated using equations of state (EoS). For nonpolar mixtures, cubic EoS provide accurate estimates of Henry's constant.[4] In this work, EoS calculations are presented for the two mixtures stated above using three different models: the Soave−Redlich−Kwong cubic EoS (SRK),[5] the cubic-plus-association EoS (CPA),[6] and the statistical-associating-fluid-theory EoS (SAFT).[7] SAFT is a statistical-mechanics-based semiempirical EoS developed specifically for systems containing chain or hydrogen-bonding molecules or both. CPA is an extension of the simple SRK EoS to hydrogen-bonding systems by accounting explicitly for association with an approach similar to SAFT. It is shown here that SRK and CPA correlate accurately the Henry's constant of methane in *n*-hexadecane but none of the three models is able to correlate accurately the Henry's constant of methane in water over the entire temperature range.

Molecular simulation has advanced to a powerful tool for mixture thermodynamic property calculations and for fluid structure analysis. In this way, molecular characteristics can be consistently correlated with macroscopic properties using a very small number of parameters. Recently, the Henry's constant of methane in water and of ethane in water over the temperature range of 300−570 K and pressure very close to pure water vapor pressure was calculated accurately from *NPT* (isothermal−isobaric) Monte Carlo simulation using the Widom test particle insertion approach.[8] For highly dense fluids, such as liquid water, the Widom method is impractical and very long simulations are required. More recently, two very efficient methods for chemical potential calculation were developed on the basis of staged and direct deletion of the test particle from the system,

* To whom correspondence should be addressed. E-mail: economou@mistras.chem.demokritos.gr.
[†] National Research Centre for Physical Sciences ''Demokritos''.
[‡] National Technical University of Athens.
[§] University of Patras.

10.1021/jp010426f CCC: $20.00
Published on Web 07/21/2001

hereafter referred to as the staged particle deletion (SPD) and direct particle deletion (DPD) methods, respectively.[9,10] These methods are used here in the course of *NPT* simulation of methane in water. Water is modeled using a two-body potential.[11] The excess chemical potential of methane infinitely diluted in water is calculated, as well as the free energy of cavity formation in water and the free energy of converting a methane molecule to a cavity (hard sphere) in water.

Furthermore, SPD *NPT* Monte Carlo simulations are reported for a light gas dissolved in a nonpolar solvent. The specific mixture examined is methane dissolved in ethane. Simulations are performed at the same reduced temperature at the saturation point of the solvent for each of the two solvents (water and ethane), so a direct comparison is possible.

Simulation data are used to develop some insight into the hydrophobic phenomenon (hydration process). In the past, hydrophobicity was associated with the very low hydrocarbon solubility in water. Furthermore, the iceberg model was used widely to explain the structure of water molecules surrounding a small solute molecule.[12,13] It has been postulated that there is an unfavorable entropy contribution to the dissolution of hydrocarbon molecules in water related to the formation of a cavity in the solvent in order to host the solute molecules. This unfavorable entropy was attributed to the small size of water molecules that results in a large number of relatively small cavities that prohibit solute molecule insertion[14−16] or to the strong hydrogen bonds formed by water molecules.[17−19] Simulation results presented here for the dissolution of methane in water and in ethane offer new insights in this area. We define two types of cavities in water, the "polar" and the "nonpolar" cavity, on the basis of the type of molecule removed for the formation of the cavity. Simulation data are analyzed, and an evaluation of the free energy of cavity formation is made for different mixtures. Finally, it is shown that the weak energetic interactions are primarily responsible for the low methane solubility in water.

Henry's Law Constant Analysis

The Henry's law constant of a solute in a solvent ($H_{\text{solute}\rightarrow\text{solvent}}$) is given by the expression

$$H_{\text{solute}\rightarrow\text{solvent}} = \lim_{x_{\text{solute}}\rightarrow 0}\left(\frac{f_{\text{solute}}}{x_{\text{solute}}}\right) \tag{1}$$

where x_{solute} is the mole fraction of the solute and f_{solute} is the fugacity of the solute. With the use of standard thermodynamic relations, eq 1 can be written as

$$\begin{aligned} H_{\text{solute}\rightarrow\text{solvent}} &= \lim_{x_{\text{solute}}\rightarrow 0}\left(\frac{\rho_{\text{solution}}}{\beta}\exp(\beta\mu^{\text{ex}}_{\text{solute}})\right) \\ &= \frac{\rho_{\text{solvent}}}{\beta}\exp(\beta\mu^{\text{ex},\infty}_{\text{solute}}) \\ &= \frac{\rho_{\text{solvent}}}{\beta}\exp(\beta\mu^{\text{ex,cav}}_{\text{solute}} + \beta\mu^{\text{ex,en}}_{\text{solute}}) \\ &= H^{\text{ideal}}H^{\text{excess}} \end{aligned} \tag{2}$$

where ρ_{solvent} is the number density of the pure solvent at a given temperature (T) and pressure (P), $\beta = 1/(k_B T)$, $\mu^{\text{ex}}_{\text{solute}}$ is the solute excess chemical potential, and $\mu^{\text{ex},\infty}_{\text{solute}}$ is the same at infinite dilution. The excess chemical potential, μ^{ex}, of a species in a mixture is defined as the chemical potential of the species at a given temperature, density, and composition minus the ideal gas chemical potential of the pure species at the temperature and molecular density it has in the mixture. In the rest of the paper, when we refer to excess chemical potential, we imply that it is at infinite dilution, unless otherwise stated. The excess chemical potential can be divided further into two terms: $\mu^{\text{ex,cav}}_{\text{solute}}$ is the free energy for the formation of a cavity in the solvent with prescribed size which is chosen at least equal to the hard core diameter of the solute molecule, and $\mu^{\text{ex,en}}_{\text{solute}}$ is the free energy of transforming the solute molecule to such a cavity (mainly due to the energetic interactions of the solute molecule with the solvent molecules). Both $\mu^{\text{ex,cav}}_{\text{solute}}$ and $\mu^{\text{ex,en}}_{\text{solute}}$ are at infinite dilution. In eq 2, the Henry's constant is written as a product of two terms: $H^{\text{ideal}} = \rho_{\text{solvent}}/\beta$ which has dimensions of pressure and is a function of pure solvent properties (and thus it is the same for all solutes dissolved in a solvent at the same conditions) and H^{excess} which is dimensionless and a measure of the nonideal solvent−solute interactions (cavity formation and energetic interactions). Most of the work presented here focuses on this nonideal contribution.

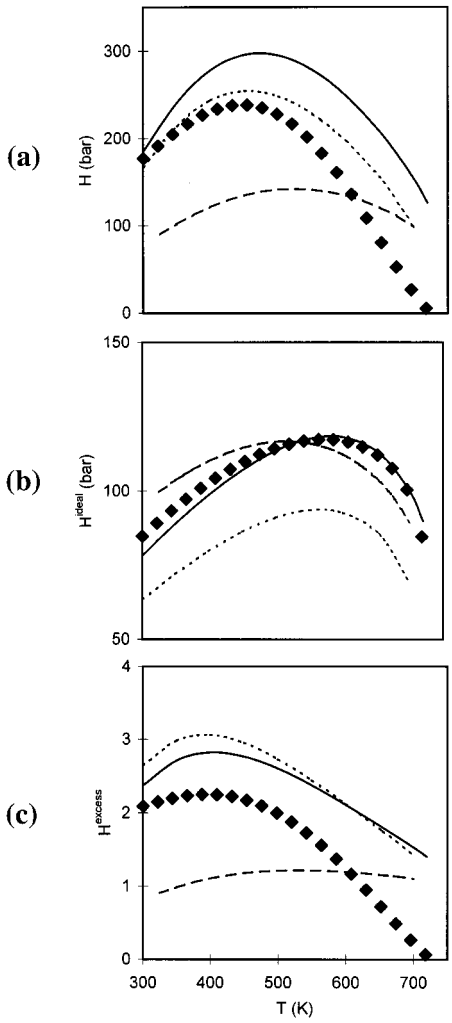

Figure 1. Henry's constant (a), H^{ideal} (b), and H^{excess} (c) of methane in *n*-hexadecane. In all cases, experimental data (◆)[3] and SRK (short dashed lines), CPA (solid lines), and SAFT (long dashed lines) predictions are shown.

In Figures 1a and 2a, experimental data[3] for the Henry's constant of methane in saturated liquid *n*-hexadecane and of methane in saturated liquid water, respectively, are shown as a function of temperature. In both cases, a maximum value is observed at temperatures well below the solvent critical tem-

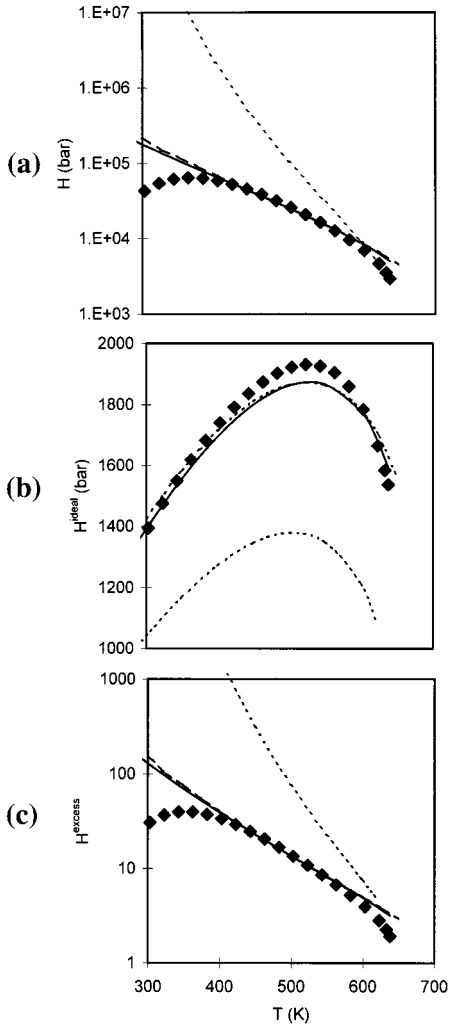

Figure 2. Henry's constant (a), H^{ideal} (b), and H^{excess} (c) of methane in water. In all cases, experimental data (◆)[3] and SRK (short dashed lines), CPA (solid lines), and SAFT (long dashed lines) predictions are shown.

perature of 722 K for *n*-hexadecane and 647.1 K for water. In Figures 1b and 2b, the H^{ideal} for the two systems is shown. In all cases, it exhibits a maximum value driven by the combined variation of saturated liquid density of the pure solvent (which in general decreases monotonically as temperature increases, with the exception of water that has a maximum saturated liquid density at 277.15 K) and the temperature (eq 2). Finally, in Figures 1c and 2c, the H^{excess} for the two mixtures is presented. The maximum values of H^{excess} in both cases are observed at temperatures close to the temperatures where *H* has a maximum. In other words, the location of the maximum in the Henry's constant value is controlled mainly by the nonidealities of mixing between solvent and solute. As one expects, H^{excess} values for methane in *n*-hexadecane are more than an order of magnitude lower than those for methane in water.

Equation of State Predictions

Calculations for the Henry's constant were performed using three EoS. SRK[5] is a cubic EoS used widely for fluid phase equilibrium calculations. SRK parameters are evaluated from the critical temperature (T_c), critical pressure (P_c), and acentric factor (ω) of the pure components. CPA[6] is an extension of the SRK that accounts explicitly for hydrogen-bonding interactions using appropriate expressions. Finally, SAFT[7] is a statistical-mechanics-based EoS developed for chain molecules and associating fluids using first-order thermodynamic perturbation theory. Detailed mathematical expressions for these equations can be found in the original publications and are not repeated here. Both CPA and SAFT are three-parameter EoS for pure nonassociating fluids and five-parameter EoS for pure associating fluids (i.e., water, alcohols, etc.). These parameters are fitted to experimental vapor pressure and liquid density data over a wide temperature range. Parameter values for the components examined in this work are shown in Tables 1 and 2.

TABLE 1: CPA Parameters for the Components Examined in This Work[a]

component	*b* (L/mol)	α_0 (bar L^2/mol)	c_1
water	0.0146	0.801	1.751
methane	0.0284	2.278	0.444
hexadecane	0.2961	94.919	1.373

[a] For water, $\epsilon^{AB} = 1793.6$ K and $\beta^{AB} = 0.1151$.

TABLE 2: SAFT Parameters for the Components Examined in This Work[a]

component	*m*	v^{00} (cm^3/mol)	u^0/k (K)
water	2.853	3.304	167.10
methane	0.996	21.475	190.72
hexadecane	11.366	11.622	209.90

[a] For water, $\epsilon/k = 1634.7$ K and $\kappa = 0.3374$.

The models are extended to mixtures using the standard van der Waals one-fluid mixing rules. For mixtures of components of considerable difference in energetic interactions (for example, a polar−nonpolar mixture), a binary parameter, k_{ij}, is used that is fitted to mixture data. For the case of methane in *n*-hexadecane, both components are nonpolar and so no binary parameter was used. In Figure 1, calculations from the three models are shown for methane in *n*-hexadecane. Interestingly, SRK predictions are in the relatively best agreement with the experimental data because of cancellation of errors. SAFT predictions for *H* are too low by a factor of 2 approximately at low temperatures and higher than the experimental values as one approaches the solvent critical point (at 722 K). Furthermore, SAFT predicts an H^{excess} value close to 1 (Figure 1c) throughout the temperature range examined, which means that $\beta\mu^{ex}$ is predicted to be close to zero. From these calculations, one may conclude that SAFT is not accurate in predicting the infinite dilution properties of light hydrocarbons in heavy hydrocarbons.

Water−methane is a highly nonideal mixture, and therefore, a binary parameter is required. Recently,[20] SAFT and CPA were tested extensively for the correlation of binary water−*n*-alkane low- and high-pressure phase equilibria and corresponding binary parameters were evaluated. For the case of water−methane, $k_{ij} = 0.495$ for SAFT and 0.05 for CPA. A similar analysis was performed for SRK, and it was found that $k_{ij} = 0.55$. These parameters were used for the calculation of the Henry's constant of methane in water shown in Figure 2. SAFT and CPA predictions agree with the experimental data only at high temperatures. As the temperature lowers below 400 K, both EoS predict that *H* and H^{excess} increase monotonically, whereas the experimental data go through a maximum and then decrease. Such deficiency of EoS for water−*n*-alkane mixtures has been also reported previously[21] and is attributed to the mean-field nature of the macroscopic models, which fail to account for the perturbation of the local structure of water induced by the insertion of the solute molecule.

Monte Carlo Simulation

Simulation Details. Henry's law constant in water and in nonpolar solvents is investigated further through Monte Carlo simulations. For all of the components examined here, two-body potential models are used. Water is modeled using the modified extended simplified point charge (MSPC/E) model that consists of a Lennard-Jones sphere (with $\epsilon/k = 74.5$ K and $\sigma = 3.116$ Å) located on the oxygen atom, two positive partial charges (each equal to $0.4108e$) located on the hydrogen atoms (at 0.9839 Å from the oxygen atom), and one negative partial charge of $0.8216e$ located on the oxygen atom.[11] The H−O−H angle is 109.47°. MSPC/E was parametrized to provide accurate vapor pressure and liquid density values of pure water at subcritical conditions. The intermolecular potential is calculated from the expression

$$u(r) = 4\epsilon\left[\left(\frac{\sigma}{r}\right)^{12} - \left(\frac{\sigma}{r}\right)^{6}\right] + \sum_{\gamma=1}^{3}\sum_{\delta=1}^{3}\frac{q_\gamma q_\delta}{r_{\gamma\delta}} \tag{3}$$

where r is the distance between the two oxygen centers and the indices γ and δ run over all charges on the molecules. Methane and ethane molecules are modeled with the TraPPE united-atom Lennard-Jones model.[22] For methane, $\epsilon/k = 148$ K and $\sigma = 3.73$ Å, whereas for ethane, $\epsilon/k = 98$ K, $\sigma = 3.75$ Å, and the C−C bond length is equal to 1.54 Å. The standard Lorentz−Berthelot combining rules were used for the interactions between unlike molecules:

$$\epsilon_{ij} = \sqrt{\epsilon_{ii}\epsilon_{jj}} \tag{4}$$

$$\sigma_{ij} = \frac{\sigma_{ii} + \sigma_{jj}}{2} \tag{5}$$

To describe properly the long-range electrostatic forces, the Ewald summation approach was used. For the case of hydrocarbon interactions, the standard long-range correction method was used[23] by setting the cutoff distance equal to 3σ.

For the case of methane dissolved in water, 200 water molecules and a single methane molecule were simulated in the *NPT* ensemble. Simulations at five different temperatures and at pressures equal to the pure water vapor pressure were performed. Calculations were made in two stages: Initially, very long runs, up to 500×10^6 moves in the case of low temperatures, were performed in order to get good statistics in the sampling of configurations. A number of configurations were stored in the course of the run in order to calculate the chemical potential of the methane using the SPD method[9] and the DPD method[10] in a postprocessing calculation.

The SPD method relies on the simulation of an N-molecule system (system I) and an $(N-1)$-molecule system (system III) resulting from the deletion of a test molecule (here, the solute molecule). The reference system of N molecules should be able to sample the complete configurational space that the perturbed system of $N-1$ molecules samples. As a result, an intermediate system of $N-1$ molecules and a hard core molecule (system II) is introduced and the free energy difference between systems I and III is calculated on the basis of the free energy differences for the pairs I−II and III−II. An optimum size of the hard core molecule with respect to the size of the deleted molecule that is system dependent and is determined early in the simulation exists.[9] Finally, $\beta\mu^{ex}_{solute}$ and its constituent cavity term and energetic term in the *NPT* ensemble are calculated from the expression

$$\beta\mu^{ex} = \beta\mu^{ex}_{energy} + \beta\mu^{ex}_{volume}$$
$$= -\ln\left(\left\langle\frac{1}{V}\right\rangle_{N,P,T}\left\langle\frac{1}{\frac{\prod_{i=1}^{N-1}H(r_{i,N})\exp(\beta U^{(N)}(\vec{r}_1,...,\vec{r}_N))}{V}}\right\rangle_{N,P,T}\right) - \ln\left(\left\langle\prod_{i=1}^{N-1}H(r_{i,N})\right\rangle_{N-1,P,T}\right) \tag{6}$$

where $H(r_{i,N})$ is a Heaviside step function and $U^{(N)}(\vec{r}_1,...,\vec{r}_N)$ stands for the intermolecular energy felt by the Nth molecule because of its interactions with the remaining $N-1$ molecules of the system. It is clear from eq 6 that the analysis presented here invokes calculations in an ensemble of N molecules and an ensemble of $N-1$ molecules with all other parameters being the same. Although in the thermodynamic limit, there is no difference between the two ensembles, special attention should be paid in the case of molecular simulation of finite size systems. A rigorous approach would require two separate simulations. However, when calculations are performed in the *NPT* ensemble, the difference between the $(N-1)$- and N-ensembles corresponds only to a weak size effect, whereas for calculations in the *NVT* ensemble, there is a small density difference. Practically, there is no difference between the two-separate-simulation calculation (referred to as SPD) and the single-simulation calculation (referred to as DPD), as will be made clear in the results section.

A number of *NVT* runs were made in order to identify the Henry's constant variation with temperature at constant volume. All of the production runs started from well-equilibrated configurations. Detailed results from the simulations are shown in Table 3 for the *NPT* simulation of methane in water, Table 4 for the *NPT* simulation of methane in ethane, and Table 5 for the *NVT* simulation of methane in water.

For the case of methane dissolved in ethane, a system of 300 ethane molecules and a single methane molecule was simulated. In this case, a much smaller number of simulation steps was used, on the order of 20×10^6 moves. Simulations for both mixtures were performed at the same reduced temperature with respect to the solvent critical temperature, so results for the two mixtures are directly comparable.

In the DPD methodology, a key variable is the distance between the center of the cavity and the solvent atom(s). This variable depends on the solvent hard core size. Special attention should be paid when comparing different systems (either with respect to solvent or with respect to solute). In the case of aqueous mixtures, the hard core of a water molecule is larger for the case of a nonpolar solute than for the case of a polar solute.

In this work, the radius of the spherical cavity, R_c, is defined as the distance from the cavity center to the center of the solvent molecule, d_{12}, minus one-half of the minimum distance that two solvent molecules can approach each other, r_{11}^{min} (see Figure 3). Here the minimum value for d_{12}, denoted as d_{12}^{min}, is set equal to the distance of closest approach between solute and solvent molecules, determined from the corresponding pair distribution function.

In the case of a nonpolar solute dissolved in water, the water molecules look larger to the nonpolar solute molecules because of the much weaker interactions between the two components. This difference is reflected in the scheme shown in the lower right part of Figure 3 where r_{11}^{min*} is larger than r_{11}^{min}. For the

TABLE 3: *NPT* Monte Carlo Simulation of Methane Infinitely Dilute in Water[a]

temp (K)	pressure (bar)	SPD $\beta\mu^{ex}_{solute}$	DPD $\beta\mu^{ex}_{solute}$	DPD $\beta\mu^{ex,en}_{solute}$	DPD $\beta\mu^{ex,cav}_{solute}$
300	0.02	3.80 ± 0.33	3.27 ± 0.25	-4.34 ± 0.13	7.61 ± 0.29
333	0.14	3.70 ± 0.18	3.83 ± 0.44	-3.69 ± 0.18	7.52 ± 0.40
371	0.80	3.58 ± 0.11	3.58 ± 0.11	-3.17 ± 0.12	6.75 ± 0.16
400	2	3.30 ± 0.05	3.38 ± 0.07	-2.83 ± 0.03	6.21 ± 0.07
470	15	2.48 ± 0.18	2.64 ± 0.19	-2.23 ± 0.15	4.50 ± 0.08

[a] The nonpolar cavity radius is $R_c = 1.79$ Å.

TABLE 4: *NPT* Monte Carlo Simulation of Methane Infinitely Dilute in Ethane[a]

temp (K)	pressure (bar)	Widom $\beta\mu^{ex}_{solute}$	SPD $\beta\mu^{ex}_{solute}$	SPD $\beta\mu^{ex,en}_{solute}$	SPD $\beta\mu^{ex,cav}_{solute}$
125	0.013	-4.11 ± 0.49	-3.84 ± 0.84	-13.41 ± 0.84	9.56 ± 0.04
150	0.91	-2.93 ± 0.18	-2.92 ± 0.49	-10.83 ± 0.49	7.91 ± 0.07
200	3	-1.83 ± 0.05	-1.99 ± 0.14	-7.42 ± 0.13	5.43 ± 0.06
250	17	-1.25 ± 0.04	-1.21 ± 0.09	-4.86 ± 0.05	3.65 ± 0.07

[a] The nonpolar cavity radius is $R_c = 1.79$ Å.

TABLE 5: *NVT* Monte Carlo Simulation of Methane Infinitely Dilute in Water at 1.062 g/cm^3 [a]

temp (K)	$\beta\mu^{ex}_{solute}$	$\beta\mu^{ex,en}_{solute}$	$\beta\mu^{ex,cav}_{solute}$
300.13	4.66 ± 0.33	-4.61 ± 0.21	9.27 ± 0.25
371.15	6.11 ± 0.19	-3.34 ± 0.15	9.44 ± 0.13
470.13	7.22 ± 0.16	-2.41 ± 0.04	9.63 ± 0.16

[a] All chemical potential calculations are from DPD. The nonpolar cavity radius is $R_c = 1.82$ Å.

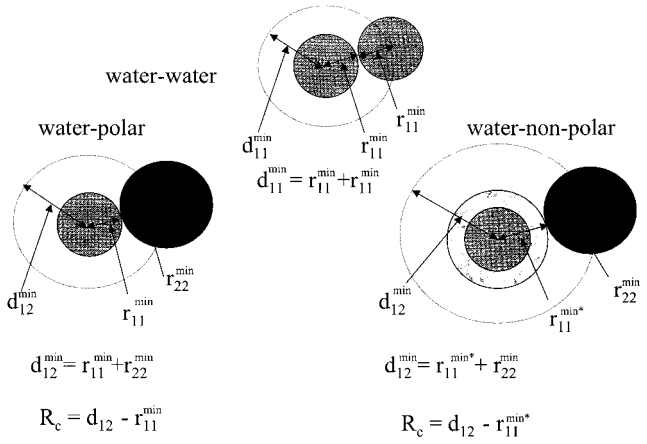

Figure 3. Schematic representation of the various size parameters used in this work: d_{ij}^{min} is the minimum distance between two molecules i and j, r_{ii}^{min} is the contribution to the minimum distance due to molecule i, and R_c is the cavity radius.

systems examined here, it is $r^{min}_{water-water} = 1.14$ Å, whereas $r^{min*}_{water-water} = 1.23$ Å.

In the simulations performed in this work, the minimum distance between different molecule pairs is $d^{min}_{water-water} \approx 0.74\sigma_{water-water}$, $d^{min}_{water-methane} \approx 0.84\sigma_{water-methane}$, $d^{min}_{methane-methane} \approx 0.86\sigma_{methane-methane}$, $d^{min}_{methane-ethane} \approx 0.87\sigma_{methane-ethane}$, and $d^{min}_{ethane-ethane} \approx 0.83\sigma_{ethane-ethane}$. The difference between $d^{min}_{water-water}$ and $d^{min}_{methane-methane}$ with respect to the corresponding σ values clearly reflects the strong effect of polar interactions between water molecules on the water hard core diameter compared to the weak interactions between methane molecules. Furthermore, the $d^{min}_{water-methane}$ value shows that the partial charges in the solvent molecule have a very weak effect on the hard core distance between a nonpolar molecule and a water molecule. Note that this is not to be expected for the case of polar molecules dissolved in water.

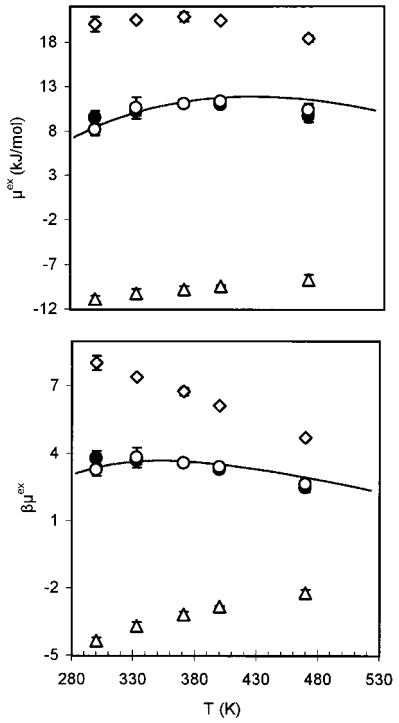

Figure 4. Excess chemical potential (top) and reduced excess chemical potential (bottom) of methane in water: experimental data (line)[3] and Monte Carlo simulation results using the SPD method[9] (●) and the DPD method[10] (○). Monte Carlo simulations are shown for the cavity formation contribution (◇) and the energetic contribution (△) for each diagram. The radius of the nonpolar cavity is $R_c = 1.79$ Å.

From the above arguments, it is clear that the accessible volume for nonpolar molecules dissolved in water is much smaller compared to the accessible volume for polar molecules, and thus, the insertion of nonpolar molecules requires larger d^{min} values compared to the insertion of polar molecules of the same size. In the literature, it has been proposed to set the hard core diameter of the solute molecule equal to the Lennard-Jones σ parameter of the solvent.[15] Although such a definition may be reasonable for the case of nonpolar solutes in water, it is highly unphysical for polar solute molecules, including water itself.

Discussion of Results. The infinite dilution chemical potential of methane in water and in ethane along the saturation curve of the solvent was calculated using the SPD method[9] and the DPD method.[10] In Table 3 and in Figure 4, experimental data and simulation results are shown for μ^{ex} and $\beta\mu^{ex}$ of methane in water. The two different sets of calculations agree with each other within statistical uncertainty, and the statistical errors are similar. Furthermore, simulation results are shown for the cavity and energy terms. Both $\beta\mu^{ex,cav}_{methane}$ and $\beta\mu^{ex,en}_{methane}$ show a monotonic variation with density, whereas their combination results in a maximum value for $\beta\mu^{ex}_{methane}$.

Molecular simulation was used to calculate the infinite dilution chemical potential of methane in a light, nonpolar solvent, namely ethane. Simulations were performed at the same reduced temperature for ethane as that for water, along the saturation curve of ethane. In this way, direct comparison can be made between the aqueous solvent and the organic solvent for the different structural and thermodynamic phenomena observed. In Figure 5, μ^{ex} and $\beta\mu^{ex}$ of methane in ethane are shown at different temperatures from the Widom insertion

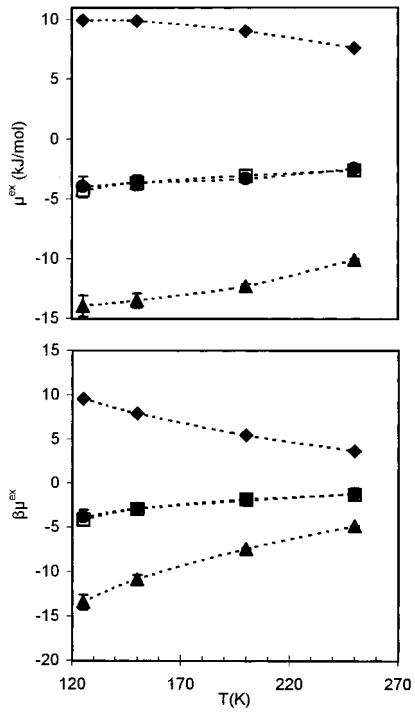

Figure 5. Excess chemical potential (top) and reduced excess chemical potential (bottom) of methane in ethane: Monte Carlo simulation results using the Widom insertion technique (□) and the SPD scheme[9] (●). Monte Carlo simulations are shown for the cavity formation contribution (◆) and the energetic contribution (▲) in each diagram. Dashed lines connect the simulation points and are drawn to guide the eye.

method and the SPD method. Calculations based on the use of the two methods are in very good agreement. It should be noted that, in the temperature range examined, $\beta\mu^{ex}_{solute}$ is a monotonic function of temperature. However, at higher temperatures approaching the critical point of ethane, $\beta\mu^{ex}_{solute}$ decreases with infinite slope at the critical point.[24]

Analysis of the Hydrophobic Phenomenon. The separation of $\beta\mu^{ex}$ into a cavity formation term and a dispersion energy term (eq 2) provides useful insight into the hydrophobic phenomenon, which is of immense importance to biology, chemistry, and physics. A number of experimental and theoretical investigations have been published concerning the hydrophobic effect. Despite this effort, a number of important issues related to this phenomenon are still unresolved. It has been claimed that the free energy for a cavity formation is much higher for the case of water compared to that for an organic solvent either because of the small size of the water molecules,[14−16] which results in the formation of several small cavities instead of a few large ones,[25−28] or because of the ordering of water molecules around the cavity.[17−19,25−28]

To obtain more meaningful results, comparisons for the different solvents (aqueous versus organic) should be made for the same thermodynamic conditions, i.e., comparison of the reduced chemical potential for the same reduced temperature at saturation. In this work, simulations for methane in the two solvents (water and ethane) were performed at saturation for the same reduced temperatures with respect to the solvent critical temperature. In Figure 6, simulation results for $\beta\mu^{ex}_{solute}$, $\beta\mu^{ex,cav}_{solute}$, and $\beta\mu^{ex,en}_{solute}$ are presented. It is clear that $\beta\mu^{ex,cav}_{solute}$ for a "nonpolar" cavity in water is close to that for a cavity of equal radius in ethane for all temperatures. There is a difference in the temperature dependence of $\beta\mu^{ex,cav}_{solute}$ in water and in ethane (not very clearly shown in Figure 6) which is due to the unique temperature dependence of water saturation density.[27,28]

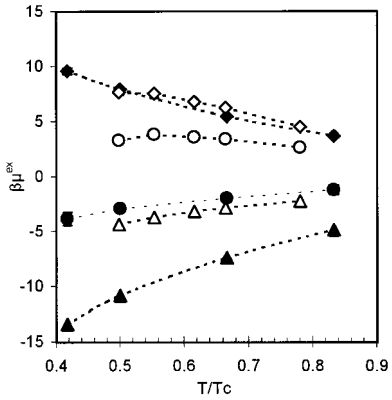

Figure 6. $\beta\mu^{ex}_{solute}$ (○), $\beta\mu^{ex,cav}_{solute}$ (◇), and $\beta\mu^{ex,en}_{solute}$ (△) of methane (for radius of the nonpolar cavity $R_c = 1.79$ Å) infinitely dilute in water from DPD and $\beta\mu^{ex}$(●), $\beta\mu^{ex,cav}_{solute}$ (◆), and $\beta\mu^{ex,en}_{solute}$ (▲) of methane in ethane from SPD at saturation. T/T_c is the reduced temperature with respect to the solvent critical temperature from the molecular model. Dashed lines connect the simulation points and are drawn to guide the eye.

Simulation results shown in Figure 6 verify that the absolute value of $\beta\mu^{ex,en}_{solute}$ is much lower for the case of water compared to the case of ethane. This leads to very high values for $\beta\mu^{ex}_{solute}$ and, consequently, for H of methane in water. In other words, simulation results support the idea that intermolecular interactions are, to a large extent, responsible for the low solubility of methane in water compared to that of methane in an organic solvent such as ethane, under corresponding thermodynamic conditions. It should be emphasized here that $\beta\mu^{ex,en}_{solute}$ is a free energy term that accounts for both energetic and entropic contributions.

The relatively small intermolecular energetic interactions can be easily explained by comparing the Lennard-Jones ϵ/k parameter value used for the various components, which is a measure of the dispersion interactions: $\epsilon/k = 74.5$ K for water, $\epsilon/k = 148$ K for methane, and $\epsilon/k = 98$ K for ethane. Although polarizability effects are not accounted for explicitly in the model, it is not expected that they would affect these results considerably.

The difference in $\beta\mu^{ex,en}_{solute}$ between methane dissolved in water and methane dissolved in ethane can be explained also on the basis of the iceberg model.[12] According to this model, the highly structured water molecules around a central methane molecule result in a lower entropic contribution to the $\beta\mu^{ex,en}_{solute}$ (dissolution becomes less favorable) compared to the case of an organic solvent.

Although the exact values for $\beta\mu^{ex,en}_{solute}$ and $\beta\mu^{ex,cav}_{solute}$ depend on the definition of the hard core radius of the solvent,[14−15,17,25−28] Figure 6 clearly demonstrates that the "energetic" term is mostly responsible for the difference in $\beta\mu^{ex}_{solute}$ values for the case of water solvent and ethane solvent.

Temperature Dependence of $\beta\mu^{ex}_{solute}$. From the analysis of experimental data for methane in water and in *n*-hexadecane, it was made clear that the variation of $\beta\mu^{ex}_{solute}$ with temperature exhibits a maximum value, at least for the case where the solvent is at (or close to) saturation. To examine the effect of density, simulations for methane in water were performed at different temperatures by keeping the water density constant at 1.062 g/cm^3. In Table 5 and Figure 7, simulation results are presented for $\beta\mu^{ex}_{solute}$, $\beta\mu^{ex,cav}_{solute}$, and $\beta\mu^{ex,en}_{solute}$ from the SPD method. Interestingly, constant density calculations exhibit a monotonic increase for $\beta\mu^{ex}_{solute}$, unlike the calculations along the solvent saturation curve. This behavior supports previous macroscopic

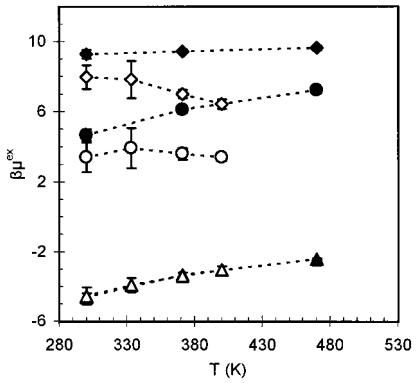

Figure 7. $\beta\mu^{ex}_{solute}$ (● and ○), $\beta\mu^{ex,cav}_{solute}$ (◆ and ◇), and $\beta\mu^{ex,en}_{solute}$ (▲ and △) of methane infinitely dilute in water at saturation conditions (open symbols) and at constant density (full symbols). The radius of the nonpolar cavity is $R_c = 1.82$ Å.

calculations by Prausnitz and co-workers.[29] Furthermore, $\beta\mu^{ex,en}_{solute}$ for a given temperature is practically independent of the density. As expected, the difference is considerable in the case of the cavity formation term. The free energy of cavity formation is a strong function of the density and is practically independent of the temperature, at least for the temperature range examined. In general, $\beta\mu^{ex,cav}_{solute}$ and $\beta\mu^{ex,en}_{solute}$ vary monotonically with density. For the case in which calculations are performed at solvent saturation, the temperature dependence of $\beta\mu^{ex,en}_{solute}$ dominates the temperature dependence of $\beta\mu^{ex}_{solute}$ at low temperatures. As temperature increases, the cavity formation term becomes progressively more important as a result of the considerable density decrease and so $\beta\mu^{ex}_{solute}$ goes through a maximum and then decreases.

Conclusions

A thorough analysis of experimental data for the Henry's constant of methane in water and in *n*-hexadecane with respect to an ideal and an excess contribution was presented. It was shown that macroscopic models such as cubic EoS predict adequately the Henry's constant of light gases in heavy nonpolar solvents, as, for example, in the case of methane in *n*-hexadecane. However, in the case of aqueous solvents, EoS are incapable of predicting accurately the experimental data over the entire temperature range.

Molecular simulation was used to evaluate the free energy of cavity formation and the free energy of solute particle to cavity transformation for the case of methane in water and of methane in ethane. These two contributions provide the excess Henry's constant. It was shown that the free energy of cavity formation for cavity sizes on the order of the size of a methane molecule in water and in ethane solvents at the same reduced temperature is surprisingly close for the case of a "nonpolar" cavity in water and that of an equal radius cavity in ethane. For a "polar" cavity, the cost is lower because water molecules appear to interact with polar molecules with a significantly smaller hard core diameter. The lack of strong energetic interactions between water and nonpolar solutes results in small negative $\beta\mu^{ex,en}_{solute}$ values that are not sufficient to overcome the unfavorable highly positive $\beta\mu^{ex,cav}_{solute}$ values. This analysis supports the argument that hydrophobic hydration is driven to a large extent by the energetic interactions between water and nonpolar solutes.

Acknowledgment. G.C.B. would like to acknowledge the support of the European Commission through Training and Mobility of Researchers (TMR) Grant No. ERB FMGE CT950051 (the Training and Research an Advanced Computing Systems (TRACS) Programme at Edinburgh Parallel Computing Centre (EPCC) and the central computing center of the National Technical University of Athens, Greece. Professor J. M. Prausnitz, University of California at Berkeley, is acknowledged for helpful discussions and suggestions.

References and Notes

(1) Tsonopoulos, C.; Wilson, G. M. *AIChE J.* **1983**, *29*, 990.
(2) Prausnitz, J. M.; Lichtenthaler, R. N.; de Azevedo, E. G. *Molecular Thermodynamics of Fluid-Phase Equilibria*, 3rd ed.; Prentice Hall: Englewood Cliffs, NJ, 1999.
(3) Harvey, A. H. *AIChE J.* **1996**, *42*, 1491.
(4) Schulze, C.; Donohue, M. D. *Fluid Phase Equilib.* **1998,** *142*, 101.
(5) Soave, G. *Chem. Eng. Sci.* **1972**, *27*, 1197.
(6) Kontogeorgis, G. M.; Voutsas, E. C.; Yakoumis, I. V.; Tassios, D. P. *Ind. Eng. Chem. Res.* **1996**, *35*, 4310.
(7) Huang, S. H.; Radosz, M. *Ind. Eng. Chem. Res.* **1990**, *29*, 2284.
(8) Errington, J. R.; Boulougouris, G. C.; Economou, I. G.; Panagiotopoulos, A. Z.; Theodorou, D. N. *J. Phys. Chem. B* **1998**, *102*, 8865.
(9) Boulougouris, G. C.; Economou, I. G.; Theodorou, D. N. *Mol. Phys.* **1999**, *96*, 905.
(10) Boulougouris, G. C.; Economou, I. G.; Theodorou, D. N. Submitted for publication.
(11) Boulougouris, G. C.; Economou, I. G.; Theodorou, D. N. *J. Phys. Chem. B* **1998**, *102*, 1029.
(12) Ben-Naim, A. *Water and Aqueous Solutions*; Plenum Press: New York, 1974.
(13) Guillot, B.; Guissani, Y. *J. Chem. Phys.* **1993**, *99*, 8075.
(14) Lee, B. *Biophys. Chem.* **1994**, *51*, 271.
(15) Madan, B.; Lee, B. *Biophys. Chem.* **1994**, *51*, 279.
(16) Matyushov, D. V.; Schmid, R. *J. Chem. Phys.* **1996**, *105*, 4729.
(17) Prevost, M.; Oliveira, I. T.; Kocher, J.-P.; Wodak, S. J. *J. Phys. Chem.* **1996**, *100*, 2738.
(18) Wallqvist, A.; Covell, D. G. *Biophys. J.* **1996**, *71*, 600.
(19) Silverstein, K. A. T.; Haymet, A. D.; Dill, K. A. *J. Am. Chem. Soc.* **1998**, *120*, 3166.
(20) Voutsas, E.; Boulougouris, G. C.; Economou, I. G.; Tassios, D. P. *Ind. Eng. Chem. Res.* **2000**, *39*, 797.
(21) Economou, I. G.; Tsonopoulos, C. *Chem. Eng. Sci.* **1997**, *52*, 511.
(22) Martin, M. G.; Siepmann, J. I. *J. Phys. Chem. B* **1998**, *102*, 2569.
(23) Frenkel, D.; Smit B. *Understanding Molecular Simulation*; Academic Press: New York, 1996.
(24) Chang, R. F.; Levelt Sengers, J. M. H. *J. Phys. Chem.* **1986**, *90*, 5921.
(25) Pratt, L. R.; Pohorille, A. *Proc. Natl. Acad. Sci. U.S.A.* **1992**, *89*, 2995.
(26) Hummer, G.; Garde, S.; Garcia, A. E.; Paulaitis, M. E.; Pratt, L. R. *J. Phys. Chem. B* **1998**, *102*, 10469.
(27) Garcia, A. E.; Hummer, G.; Garde, S.; Paulaitis, M. E.; Pratt, L. R. *Phys. Rev. Lett.* **1996**, *77*, 4966.
(28) Hummer, G.; Garde, S.; Garcia, A. E.; Paulaitis, M. E.; Pratt L. R. *Chem. Phys.* **2000**, *258*, 349.
(29) Preston, G. T.; Funk, E. W.; Prausnitz, J. M. *Phys. Chem. Liq.* **1971**, *2*, 193.